

# HI content and other structural properties of galaxies in the Virgo cluster from the Arecibo Legacy Fast ALFA Survey

G. Gavazzi<sup>1</sup>, R. Giovanelli<sup>2</sup>, M. P. Haynes<sup>2</sup>, S. Fabello<sup>1</sup>, M. Fumagalli<sup>1</sup>, B. R. Kent<sup>2</sup>, R. A. Koopmann<sup>3</sup>, N. Brosch<sup>4</sup>, G. L. Hoffman<sup>5</sup>, J. J. Salzer<sup>6</sup>, and A. Boselli<sup>7</sup>

<sup>1</sup> Università degli Studi di Milano-Bicocca, Piazza delle Scienze 3, 20126 Milano, Italy  
e-mail: giuseppe.gavazzi@mib.infn.it

<sup>2</sup> Center for Radiophysics and Space Research and National Astronomy and Ionosphere Center, Cornell University, Ithaca, NY 14853, USA

<sup>3</sup> Dept. of Physics & Astronomy, Union College, Schenectady, NY 12308, USA

<sup>4</sup> The Wise Observatory and The Raymond & Beverly Sackler School of Physics and Astronomy, Tel Aviv University, Israel

<sup>5</sup> Hugel Science Center, Lafayette College, Easton, PA 18042, USA

<sup>6</sup> Astronomy Dept. Wesleyan University, Middletown, CT 06457, USA

<sup>7</sup> Laboratoire d'Astrophysique de Marseille, BP 8, Traverse du Siphon, 13376 Marseille, France

Received 10 January 2008 / Accepted 25 January 2008

## ABSTRACT

We report the results of an HI blind survey of 80 deg<sup>2</sup> of the Virgo cluster, based on the 08° ≤ δ ≤ 16° strip of ALFALFA, the Arecibo Legacy Fast ALFA Survey. 187 HI sources of high significance are found providing a complete census of HI sources in this region of the Virgo cluster (−1000 < cz < 3000 km s<sup>−1</sup>) with M<sub>HI</sub> ≥ 10<sup>7.5–8</sup> M<sub>⊙</sub>. 156/187 (83%) sources are identified with optical galaxies from the Virgo Cluster Catalogue (Binggeli et al. 1985, AJ, 90, 1681), all but 8 with late-type galaxies. Ten sources are not associated with optical galaxies and were found to correspond to tidally-disrupted systems (see Kent et al. 2007, ApJ, 665, L15; and Haynes et al. 2007, ApJ, 665, L19). The remaining 21 (11%) are associated with galaxies that are not listed in the Virgo Cluster Catalogue. For all sources with an optical counterpart in the Sloan Digital Sky Survey, we analyzed *i*-band SDSS plates to measure optical structural parameters. We find that in the Virgo cluster: i) HI inhabits galaxies that are structurally similar to ordinary late-type galaxies; ii) their HI content can be predicted from their optical luminosity; iii) low surface brightness galaxies have low optical luminosity and contain small quantities of neutral hydrogen; iv) low surface brightness, massive Malin1 type galaxies are comfortably rare objects (less than 0.5%); v) there are no “dark-galaxies” with HI masses M<sub>HI</sub> ≥ 10<sup>7.5–8</sup> M<sub>⊙</sub>; vi) less than 1% of early-type galaxies contain neutral hydrogen with M<sub>HI</sub> ≥ 10<sup>7.5–8</sup> M<sub>⊙</sub> (di Serego Alighieri et al. 2007, A&A, 474, 851).

**Key words.** galaxies: clusters: individual: Virgo – galaxies: evolution – galaxies: ISM – galaxies: fundamental parameters

## 1. Introduction

The faint-end slope of the halo mass function either predicted analytically (Press & Schechter 1974) ( $\alpha = -1.8$ ) or by numerical CDM simulations (e.g. Jenkins et al. 2001) ( $\alpha = -2$ ) is uncomfortably steeper than the observed slope of the optical luminosity function of galaxies (e.g. Blanton et al. 2003) ( $\alpha = -1.1$ ) (see however  $\alpha = -1.5$  in *r* band by Blanton et al. 2005). If many sterile halos (i.e. unable to give birth to stars), the so called *dark galaxies*, or many low mass galaxies with low optical surface brightness, yet retaining some neutral hydrogen existed, outnumbering the normal galaxies, the faint-end slope of the HI mass function would be steeper than that of the optical luminosity function, perhaps reconciling the observations with the theoretical predictions. However the measured faint-end slope of the HI mass function, even in its most robust determination (Springob et al. 2005) is significantly flatter ( $\alpha = -1.24$ ) than the theoretical one (see also Zwaan et al. 2001). The Zwaan et al. (2005) HI mass function, based on HIPASS (HI Parkes All-Sky Survey) data (Meyer et al. 2004), is flatter ( $\alpha = -1.37$ ) than predicted, although it suffers from statistical limitations due to the paucity of objects (40) with M<sub>HI</sub> ≤ 10<sup>8</sup> M<sub>⊙</sub> and from distance

uncertainties (Masters et al. 2004). To improve the determination of the HI mass function, several blind HI surveys have been recently carried out or are under way. HIDEEP (Minchin et al. 2003) is a deep HI survey of 32 deg<sup>2</sup> in Centaurus, carried out with the Parkes multibeam system, sensitive to M<sub>HI</sub> ≥ 10<sup>8</sup> M<sub>⊙</sub>, with deep optical follow-up plates. A more recent one that combines a large area with a high sensitivity is the 86 deg<sup>2</sup> survey in the direction of Canes Venatici (Cvn) carried out with the WSRT (Westerbork Synthesis Radio Telescope) by Kovac (2007). Incidentally the slope of the faint-end mass function derived using 70 sources with M<sub>HI</sub> ≥ 10<sup>6.5</sup> M<sub>⊙</sub> from this survey is flatter than ever ( $\alpha = -1.17$ ).

The Arecibo telescope, equipped with the new 7 beam system ALFA, has recently started a number of HI blind surveys. The Arecibo Galaxy Environment survey (AGES) (Auld et al. 2006) has covered some patches of sky, including 5 deg<sup>2</sup> of the Coma supercluster containing the cluster A1367, with a sensitivity of M<sub>HI</sub> = 10<sup>8.8</sup> M<sub>⊙</sub> at the distance of Coma (300 s integration time per beam, rms = 0.84 mJy/beam; Cortese et al. 2007). Highly statistically significant results will be obtained from ALFALFA, the Arecibo Legacy Fast ALFA Survey, that

covers the Arecibo sky (7000 deg<sup>2</sup>) in a 2-pass drift-scan mode (48 s integration, with a typical rms = 2.1 mJy/beam at 10 km s<sup>-1</sup> resolution; Giovanelli et al. 2005). Besides a robust determination of the faint-end slope of the HI mass function, (based on several hundred galaxies with  $M_{\text{HI}} \leq 10^{7.5} M_{\odot}$ ) ALFALFA will provide more evidence on whether low surface brightness galaxies, that are so elusive optically (Disney 1976; Disney & Phillipps 1987; Sabatini et al. 2003), will change our understanding of galaxies in the local universe. This issue has two aspects that could be addressed and solved with ALFALFA. One is to increase the number of dwarf galaxies surveyed to better determine the number density of low surface brightness galaxies that, in spite of their low optical visibility, are HI rich. (Galaxies of decreasing mass have an increasing gas fraction and a decreasing optical (*i*-band) surface brightness, Boselli et al. 2001; Warren et al. 2006.) The other is to confirm and corroborate the finding of Briggs (1997), Rosenberg et al. (2002), Zwaan et al. (2003), Minchin et al. (2004) that the frequency of Malin1-type galaxies, i.e. massive, gas rich objects of very low optical surface brightness, is insignificant (see also Hayward et al. 2005). Malin1 was indeed discovered in HI in the background of the Virgo cluster (Impey & Bothun 1989). How many unknown low surface brightness galaxies remain hidden in the local universe, unseen by optical observations? ALFALFA should provide the complete census of such objects.

In the last two years ALFALFA has covered most of the Virgo cluster (Giovanelli et al. 2006), the nearest rich cluster, providing ~1000 HI sources in 80 deg<sup>2</sup>, perhaps the highest space density of HI sources in the whole ALFALFA survey. The analysis of this sample will dramatically enhance our understanding of the issues outlined above. The Virgo region is especially useful because of the existence of a very deep optical catalogue of galaxies, the Virgo Cluster Catalogue (VCC) by Binggeli et al. (1985), that will allow a comparison of the properties of optically and radio selected objects in this region. The overlap between the ALFALFA survey and Goldmine, a collection of HI pointed observations in the direction of Virgo obtained by many observers during the years (Gavazzi et al. 2005), also allows a comparison of the relative quality of the two databases. These are the issues that the present paper on the Virgo cluster, as seen by ALFALFA, wishes to address. A forthcoming paper will analyze H $\alpha$  observations obtained recently of several hundred HI galaxies discovered by ALFALFA in the Virgo cluster and in its immediate surroundings (Gavazzi et al., in preparation), addressing the issue of the environmental dependence of galaxy evolution (see a review by Boselli & Gavazzi 2006) by comparing the rate of transformation of primordial gas into young stars in the Virgo cluster with that in less dense environments.

The structure of the present paper is as follows. The HI and optical selected samples are presented in Sect. 2. The data analysis is presented in Sect. 3, where the reduction of optical images taken from the Sloan Digital Sky Survey (SDSS) is discussed in detail. Section 4 gives the comparison between the results of ALFALFA and pointed observations available in the literature. The results are discussed in Sect. 5.

## 2. The sample

The present analysis is focused on the ALFALFA blind HI survey in the region of the Virgo cluster; more precisely in the area of intersection between ALFALFA, as available in Sept. 2007, and the VCC. The ALFALFA survey provides a sample of HI selected objects, and the VCC a list of optically selected galaxies.

### 2.1. The HI selected sample

The HI selected sample consists of 187 ALFALFA sources meeting the following criteria:

- i) their right ascensions lie in the interval  $12^{\text{h}}08^{\text{m}}30^{\text{s}} \leq \text{RA} \leq 12^{\text{h}}48^{\text{m}}20^{\text{s}}$  (ca.  $182^{\circ} \leq \text{RA} \leq 192^{\circ}$ ) (J2000) corresponding to the extent in RA of the VCC, and their declinations range between  $08^{\circ} \leq \delta \leq 16^{\circ}$  (J2000), i.e., they lie in the declination strip that has been fully mapped by ALFALFA. North of 12 deg the catalogued sources are taken from Giovanelli et al. (2007); for  $08^{\circ} \leq \delta \leq 12^{\circ}$  the list of sources is not yet published (Kent et al., in preparation);
- ii) they have recessional velocities in the range  $-1000 < cz < 3000$  km s<sup>-1</sup>, bracketing the full depth of the Virgo cluster (see Gavazzi et al. 1999);
- iii) they have quality Code = 1, i.e., their statistical significance is higher than  $S/N = 6.5$ . (We do not consider Code = 2 objects, i.e., sources with  $S/N < 6.5$  that have optical counterparts with optical redshifts matching the HI line redshift.)
- iv) they are not included in the circle of projected radius of 1.0 deg centered on M 87, where ALFALFA is strongly incomplete because of loss of spectral sensitivity due to the bright (220 Jy at 1415 MHz) continuum source associated with M 87;
- v) they lie outside one resolution element (3.5 arcmin) of any other strong source at similar redshift. The six excluded sources because of this criterion are:  
122140.1 +143621 = VCC0497 conf by VCC0483  
122140.1 +143621 = VCC1673 conf by VCC1676  
124331.5 +113500 = VCC1972 conf by VCC1978.

Since the mean rms of ALFALFA is 2.1 mJy/beam, the survey detection limit (for  $S/N = 6.5$ ) is 0.5 Jy/beam km s<sup>-1</sup> for typical widths of 40 km s<sup>-1</sup>, thus, at the mean distance of the Virgo cluster (17 Mpc), using the relation:

$$M_{\text{HI}} = S/N \times \text{rms} \times W \times \text{dist}^2 \times 2.36 \times 10^5 (M_{\odot}) \quad (1)$$

these sources have  $M_{\text{HI}} \geq 10^{7.5} M_{\odot}$ . The  $M_{\text{HI}}$  limit, however depends on the line width, thus on the system's mass and inclination, as detailed in Sect. 5.1, resulting in  $10^{7.5} M_{\odot} \leq M_{\text{HI limit}} \leq 10^8 M_{\odot}$ .

### 2.2. The optically selected sample

From the VCC catalogue (Goldmine version, Gavazzi et al. 2003), restricted to the region in common with ALFALFA we have extracted two subsamples of optically selected galaxies that are bona-fide Virgo cluster members, whose distances have been assigned following the subcluster membership criteria of Gavazzi et al. (1999), updated with new redshift measurements.

The VCC catalogue contains galaxies as faint as 20 mag, but is complete to  $m_B < 18$  mag, within a limiting surface brightness of 25.3 B mag arcsec<sup>-2</sup> (Binggeli et al. 1985). From this catalogue we have considered:

- Sample A (deep) consisting of 1112 galaxies with  $m_B < 20$  mag;

- Sample B (shallow) consisting of 469 galaxies with  $m_B \leq 17$  mag<sup>1</sup>, 278 of which are early-type (dE-E-S0-S0a)<sup>2</sup> and 191 are late-type (Sa-Irr-BCD) galaxies. The number of galaxies with redshifts is 410/469, including 226/278 early-types and 184/191 late-types. At the mean distance of the Virgo cluster (17 Mpc, or  $M - m = -31.1$  mag)  $m_B \leq 17$  mag corresponds to  $M_B \leq -14.1$  mag, thus even Sample B includes dwarf systems.

### 3. The data reduction

#### 3.1. HI (ALFALFA)

For each of the HI selected sources we consider the following HI parameters taken from ALFALFA (Giovanelli et al. 2007):

- the (J2000) coordinates (affected by an error that depends on  $S/N$ , with a mean of  $\approx 24$  arcsec);
- the recession velocity  $VP$ ;
- the observed width of the HI line  $W$ . This is the width of the profile measured at the 50% level of each of the two peaks, corrected for instrumental broadening;
- the total flux under the HI line:  $SintP$  ( $\text{Jy km s}^{-1}$ ).

For sources optically identified with VCC galaxies, we convert  $SintP$  into the HI mass using:  $M_{\text{HI}} = 2.36 \times 10^5 \times SintP \times (dist)^2 (M_{\odot})$ , where the distance is determined as in Gavazzi et al. (1999), otherwise using 17 Mpc, and we correct the observed line width  $W$  for projection effects, using the ratio of the optical minor-to-major axes:  $W_c = W / \sin(\arcsin(b/a))$ .

We also estimate the HI deficiency parameter following Haynes & Giovanelli (1984) as the logarithmic difference between  $M_{\text{HI}}$  of a reference sample of isolated galaxies and  $M_{\text{HI}}$  actually observed in individual objects:  $Def_{\text{HI}} = \text{Log}M_{\text{HI ref}} - \text{Log}M_{\text{HI obs}}$ .  $\text{Log}M_{\text{HI ref}}$  has been found to be linearly related to the galaxies linear diameter  $d$  as:  $\text{Log}M_{\text{HI ref}} = a + b\text{Log}(d)$ , where  $d$  (in kpc) is determined at the 25th  $B$ -band isophote, and  $a$  and  $b$  are weak functions of the Hubble type. We caution that the Haynes & Giovanelli (1984) reference sample of isolated galaxies included only relatively large ( $a > 1$  arcmin) UGC objects so that the  $Def_{\text{HI}}$  parameter is poorly calibrated for smaller objects, making determinations of the HI deficiency for the smallest objects uncertain and likely underestimated (Solanes 1996). Furthermore, as discussed in Solanes et al. (2001) galaxies in the latest Hubble types (Scd-Im-BCD), for which we have adopted  $a$  and  $b$  parameters consistent with those of Sc, are more subject to observational biases than higher surface brightness galaxies. The reader should be aware that the determinations of the HI deficiency for these objects is highly uncertain.

For all radio sources we compute the total flux divided by the line width:  $\Sigma_{\text{HIc}} = SintP/W$  in  $\text{Jy/beam}$ ; this parameter is an indicator of the “visibility” in the ALFALFA survey (see Fig. 8).

<sup>1</sup> We have preferred not to extend the shallow sample B to  $m_B = 18$  mag because in the bin  $17 \leq m_B \leq 18$  mag only 6% of the VCC galaxies have an HI counterpart in ALFALFA, while in the bin  $16 \leq m_B \leq 17$  mag 40% are in ALFALFA.

<sup>2</sup> Notice that the morphological class “dE” might be contaminated by some transition objects (dE/dIrr) but we find at most 8 gas-rich ones, as shown in Sect. 3.4.

#### 3.2. Optical and HI (Goldmine)

For each of the VCC galaxies we take from the Goldmine database:

- the (J2000) optical coordinates (accurate to  $\approx 30$  arcsec);
- the morphological type (adopted from Binggeli et al. 1985; and from Binggeli et al. 1993);
- the major ( $a$ ) and minor ( $b$ ) axes (arcmin) (from Binggeli et al. 1985). These quantities are used to correct the observed line widths according to the galaxy inclination;
- the distance (in Mpc) (computed according to the criteria of Gavazzi et al. 1999). The adopted distances for each subgroup of Virgo are:  $17 \pm 0.3$  Mpc for cluster A, the North and East clouds and the Southern extension,  $23 \pm 0.5$  Mpc for cluster B and  $32 \pm 0.9$  Mpc for the W and M clouds.

In order to compare the new HI parameters derived by ALFALFA with the plethora of earlier pointed observations, collected and made as homogeneous as possible by Gavazzi et al. (2005) for the Goldmine HI database, we also consider:

- the measured width of the HI line. The Goldmine measurement differs from that of ALFALFA, as it corresponds to the average of the line widths measured at the 20% and 50% levels of the peak intensity, uncorrected for instrumental broadening;
- the hydrogen mass  $M_{\text{HI}} = 2.36 \times 10^5 \times Sint \times (dist)^2 (M_{\odot})$  where  $Sint$  is derived from pointed 21 cm observations. It should be noted that the 21 cm data in Goldmine were obtained from a variety of observations taken at Arecibo, some of which lasted much longer (typically one hour) than the ALFALFA observations ( $\sim 48$  s in the beam), thus reaching a sensitivity about one order of magnitude better than ALFALFA. These measurements are however limited to late-type galaxies.

#### 3.3. SDSS imaging material and reduction

For the optical comparisons, we obtained  $g$  and  $i$  band images from the Sloan Digital Sky Survey (DR 5) (Adelman et al. 2007) that cover the 187 HI selected sources and the optically selected late-type galaxies with  $m_B \leq 17$  (Sample B). Only one galaxy (VCC1401) was not available the SDSS. Two or more (up to 4) SDSS fields were combined for 13 galaxies (VCC66, 89, 167, 596, 865, 873, 939, 1588, 1727, 1778, 1932, 2058 and 2070) that were present in two or more SDSS images. All frames were photometrically calibrated using the wavelength dependent parameters contained in the calibration tables associated with the individual SDSS images, namely the zero point ( $aa$ ), the extinction coefficient ( $kk$ ) and the airmass. The effective zero point (in AB magnitudes) was derived using:  $ZP_{\text{eff}} = aa + kk * \text{airmass}$ . (See the SDSS data release 6 for further details on the flux calibration.)

The SDSS image analysis was carried out in the IRAF environment and relied on the STSDAS package<sup>3</sup> and on GALPHOT (developed for IRAF- STSDAS mainly by W. Freudling,

<sup>3</sup> IRAF is the Image Analysis and Reduction Facility made available to the astronomical community by the National Optical Astronomy Observatories, which are operated by AURA, Inc., under contract with the US National Science Foundation. STSDAS is distributed by the Space Telescope Science Institute, which is operated by the Association of Universities for Research in Astronomy (AURA), Inc., under NASA contract NAS 5–26555.

J. Salzer, and M. P. Haynes and adapted by S. Zibetti and L. Cortese. See Gavazzi et al. 2001).

For each frame the sky background was determined as the mean number of counts measured in regions of “empty” sky, and it was subtracted from the frame. Sky-subtracted frames were inspected individually and the light from superposed or nearby stars and galaxies was masked.

The 2-dimensional light distribution of each galaxy was fit with elliptical isophotes, using the task *cphot*, a modified version of the STSDAS *isophote* package. Starting from a set of initial parameters given manually, the fit maintains as free parameters the ellipse center, ellipticity and position angle. The ellipse semi-major axis is incremented by a fixed fraction of its value at each step of the fitting procedure. The routine halts when the surface brightness found in a given annulus equals the sky rms. The fit fails to converge for 46 galaxies with very irregular light distributions or low surface brightness. In these cases we kept fixed one or more of the initial parameters. In 14 instances of exceedingly low brightness no reliable fit was obtained (for ten HI selected objects and for four optically selected galaxies, namely: VCC 585, 1121, 1582, 1884).

The resulting radial light profiles were fitted with models of the galaxy light distribution. The majority, 72%, were best fit with an exponential disk law, while 27% were best fit by a combination of a disk and a bulge  $r^{1/4}$  law and 1% by a pure de Vaucouleurs law (de Vaucouleurs 1948).

Total magnitudes  $g, i$  were then obtained by adding to the flux measured within the outermost significant isophote the flux extrapolated to infinity along either the exponential law that fitted the outer parts of most galaxies (pure disks and B+D galaxies), or the  $r^{1/4}$  law (dV galaxies). The mean statistical uncertainty in the determination of the total magnitude is 0.10 mag. The effective radius  $r_e$  (the radius containing half of the total light, in arcsec) and the effective surface brightness  $\mu_e$  (the mean surface brightness within  $r_e$  in mag arcsec $^{-2}$ ) of each galaxy are computed only for the  $i$  band. The mean statistical uncertainties of the determination of  $r_e$  and  $\mu_e$  are 2 arcsec and 0.15 mag arcsec $^{-2}$ , respectively. The statistical uncertainties refer to the errors obtained from fitting models to the observed galaxy light distributions; we note that they do not correlate with magnitude or surface brightness, but rather with the presence of complex structures (e.g. bars or irregularities in the light profiles). Besides the statistical uncertainties, however, the photometric parameters of faint galaxies are affected by additional uncertainties that might depend on local fluctuations of the sky brightness. In the following analysis all fits are performed with the maximum likelihood method using statistical uncertainties.

Finally we computed another structural parameter: the concentration index ( $C_{31}$ ), defined by de Vaucouleurs (1977) as the model-independent ratio between the radii that enclose 75% and 25% of the total  $i$  light.

We converted the total  $i$ -band magnitude to the stellar mass using:  $\log(M_{\text{star}}/M_{\odot}) = -0.152 + 0.518 * (g - i) + \log I$  (see Appendix A2 in Bell et al. 2003), where  $I$  is the  $i$ -band luminosity. The typical uncertainty of  $\log(M_{\text{star}}/I)$  is  $\sim 0.1$  dex.

### 3.4. The radio-optical identifications

We cross-correlated the 187 HI selected sources with the optically selected sample A (deep) to obtain the optical identifications of all HI sources matching a simple positional criterion (separation  $< 1$  arcmin). Figure 1, top panel, provides the locations of these objects. We find 156/187 (83%) identifications

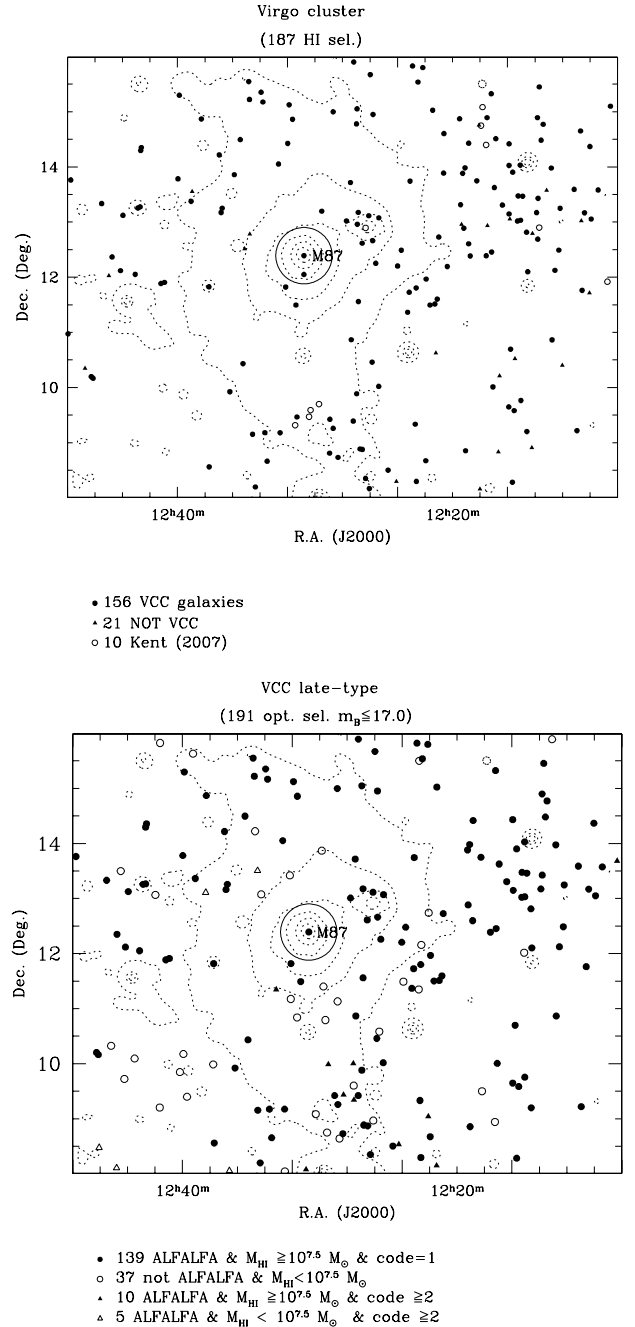


**Fig. 1.** The distribution in celestial coordinates of sources in the Virgo cluster. Contours from the X-ray ROSAT all sky survey (Böhringer et al. 1994) are given by dashed lines. The solid line shows a one degree circle centered on M 87, within which ALFALFA is complete due to the strong continuum of M 87. *Top:* ALFALFA selected sources identified with VCC galaxies with  $m_B < 20$  (filled circles). Ten non-identified sources labeled as tidally-disrupted clouds by Kent et al. (2007) (empty circles) and 21 sources identified with faint galaxies not listed in the VCC (filled triangles) are given. *Bottom:* optically selected galaxies, consisting of 191 late-type galaxies with  $m_B \leq 17$  in the VCC. 139 that have been detected by ALFALFA are plotted with filled circles, 15 that have been detected by ALFALFA with Code  $\geq 2$  with filled triangles and another 37 detected in Goldmine, but not ALFALFA (as their HI mass is  $M_{\text{HI}} < 10^{7.5} M_{\odot}$  based on Goldmine) with empty circles.

with VCC galaxies (including 8 sources associated with early type galaxies – these coincide with the Code 1 sources found by di Serego Alighieri et al. 2007). Ten of the remaining 31 sources

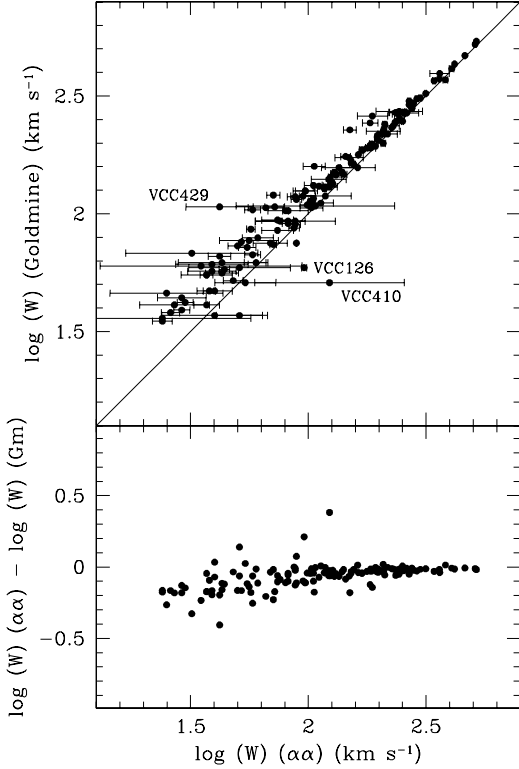


**Fig. 2.** Comparison of the ALFALFA (blind) and Goldmine (pointed) 21-cm line width measurements. The most deviant objects are labeled with their VCC names. The line represents the one to one relation.

are not associated with optical galaxies and were found to correspond to tidally-disrupted systems by Kent et al. (2007) and by Haynes et al. (2007). Among the other 21 (11% of the total sample), 15 are associated with faint galaxies that are surprisingly not listed in the VCC in spite of being clearly detected and measurable on the SDSS material. Only 6 are not visible in the SDSS images; we consider their effective surface brightness fainter than  $25 \text{ mag arcsec}^{-2}$ .

We then cross-correlated the 469 galaxies in the optically selected VCC sample B (shallow) with the ALFALFA positions, separately for the 191 late-type galaxies and for the 278 early-type galaxies. Figure 1, bottom panel, provides the locations of these objects. Only 4 matches are found with the 278 early-type galaxies of Sample B: VCC93, 209, 304 and 355. Among the late-types galaxies, 139/191 (73%) match an HI source. Thus only 52/191 (27%) late-type VCC galaxies in Sample B do not match HI selected sources. Of these, 37 lie below the sensitivity threshold of ALFALFA, based on Goldmine; the remaining 15 are not considered by us in spite of being detected, because they have Code  $\geq 2$ .

In any case most of these low  $M_{\text{HI}}$  galaxies (32/37 or 46/52 including the code  $\geq 2$ ) are relatively bright and HI deficient ( $Def_{\text{HI}} > 0.6$ ).

## 4. Analysis

### 4.1. Consistency with previous pointed HI measurements

The comparison of the line widths determined by ALFALFA and by the pointed observations collected in the Goldmine database is shown in Fig. 2. There is a tendency ALFALFA HI line widths to be up to 50% smaller than those of Goldmine for galaxies with  $W < 100 \text{ km s}^{-1}$ . The difference decreases for increasing

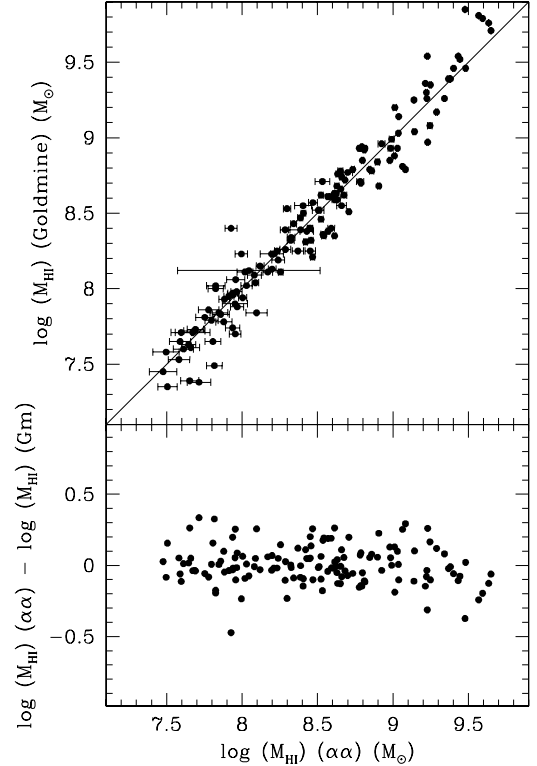


**Fig. 3.** Comparison of the ALFALFA (blind) and Goldmine (pointed) 21-cm line intensity measurements of Virgo galaxies. The line represents the one to one relation.

line widths. This discrepancy reflects the difference of the two methods used to measure the line widths in the two datasets (i.e. average of 20% and 50% of the peak intensity in Goldmine vs. 50% level of each of the two peaks in ALFALFA). The line measurements taken homogeneously by ALFALFA should provide a reliable determination of the distances to individual galaxies using the Tully-Fisher relation (see next section).

Figure 3 shows the comparison of the HI mass measurements. There is no apparent trend with  $M_{\text{HI}}$ .

### 4.2. The Tully-Fisher relation

Using the corrected line width  $W_c$  as measured by ALFALFA and the  $i$ -band luminosity derived from the total  $i_{AB}$  magnitude, and restricting to objects with inclination larger than  $35^\circ$ , we obtain the  $i$ -band Tully-Fisher relation for galaxies in the Virgo cluster (see Fig. 4). For this specific purpose it was necessary to consider a subsample of non-deficient galaxies, i.e. galaxies with the HI deficiency parameter  $Def_{\text{HI}} < 0.6$ . This is because in the ram-pressure scenario (e.g. Abadi et al. 1999) HI ablation proceeds outside-in, depleting first the gas that is less gravitationally bound, so that the full width of the measured line profile underestimates the rotational velocity. After allowing for a 0.50 mag shift for converting  $i_{AB}$  (SDSS) into  $I_J$  (Johnson) magnitudes (according to the conversion table in NED), we apply the internal extinction corrections as in Giovanelli et al. (1997). For  $\log(W_c) > 2$  and excluding the Irr/BCD galaxies, the obtained relation appears consistent in slope and zero point with the template  $I_J$  Tully-Fisher determined by Masters et al. (2006). This indicates that the distances of the individual Virgo galaxies adopted in this work are not badly determined. For  $\log(W_c) \leq 2$

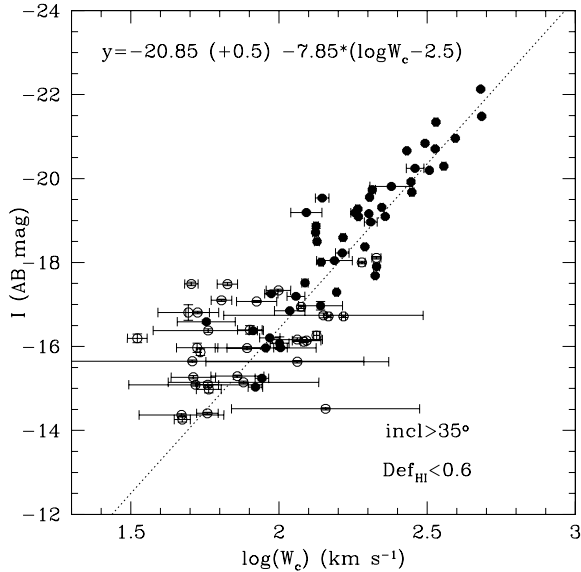


**Fig. 4.** The Tully-Fisher relation as determined with ALFALFA line widths and  $i$ -band asymptotic (AB) magnitudes, converted to  $I_J$  and corrected for internal extinction, limited to non-deficient galaxies with inclination larger than 35 deg. Filled symbols represent spiral galaxies, while empty symbols refer to Irr/BCDs. The line gives the slope of the  $I$ -band Tully-Fisher determination by Masters et al. (2006).

and for Irr/BCD the dispersion of the relation makes it useless as a distance indicator.

## 5. Discussion

### 5.1. The HI to stellar mass relation

A basic feature of galaxies is the fact that the HI mass increase with increasing optical luminosity is flatter than the direct proportionality (Roberts & Haynes 1994). Figure 5 shows the relation between these two quantities (given for all optically identified HI selected sources). Because the present analysis is carried out with galaxies belonging to a rich cluster, the study of the dependence of HI mass on luminosity must be corrected for the effects of ram-pressure stripping (that causes HI deficiency: Giovanelli & Haynes 1985) by excluding HI deficient objects ( $Def_{HI} \geq 0.6$ ). This is why galaxies with “normal” HI content are plotted separately from the HI-deficient objects in Fig. 5. (We remind the reader that the definition of HI deficiency adopted here is a diameter-, not an optical-luminosity-based relation.) The line fitted to the non-deficient objects (using the “maximum likelihood” method) shows that the slope of the relation with the optical ( $i$ -band) luminosity is  $< 1$ , with  $\log(M_{HI}/M_{\odot}) = (0.563 \pm 0.002) \times \log(I \text{ lum}) + (3.68 \pm 0.02)$ . After transforming the optical luminosity into the stellar mass (using the relation given in Sect. 3.3) the meaning of the above finding is emphasized by plotting in Fig. 6 the ratio of the HI to stellar mass versus the stellar mass itself. By focusing only on the non-deficient objects it is apparent that the most massive galaxies, the giant spirals with stellar masses in excess of  $10^{10} M_{\odot}$ , have approximately 5% of their stellar mass in gas, intermediate mass galaxies have 10% gaseous mass, but in the dwarfs the gas content can exceed the mass of the stars by a factor up to 10. Molecular hydrogen is not expected to change this trend. Using a luminosity/metallicity dependent CO to  $H_2$  conversion factor, it has been shown that the molecular gas fraction decreases with increasing stellar mass and that the  $M_{H_2}/M_{HI}$

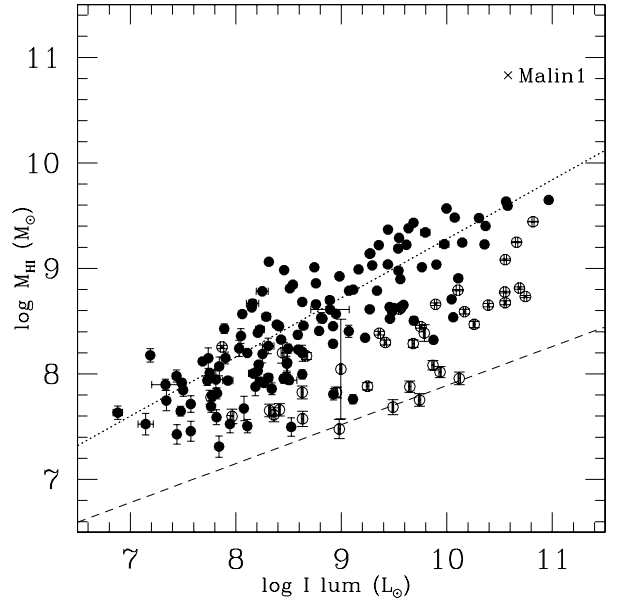


**Fig. 5.** HI/optical luminosity correlation plotted separately for non-deficient (filled dots) and for objects with  $Def_{HI} \geq 0.6$  (open symbols). The dashed line gives the (line width dependent) limit of ALFALFA computed for an inclination of 45 deg. The diagonal dotted lines represent the *maximum likelihood* regressions fitted to the non-deficient galaxies.

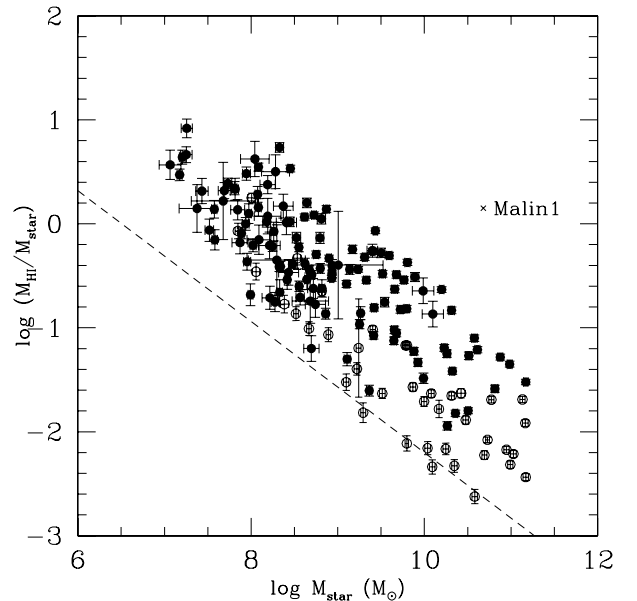


**Fig. 6.** Gas to star mass ratio separately for non-deficient (filled dots) and for objects with  $Def_{HI} \geq 0.6$  (open symbols). The dashed line represents the limit of the HI survey computed for an inclination of 45 deg.

ratio stays approximately around 15% regardless of the morphological type (see Fig. 6 in Boselli et al. 2002). The extrapolation of this relation to even lower stellar masses, suggests the existence of completely gas-dominated objects, similar to the so called “dark galaxies”. One of the results of ALFALFA is however that, at least in the mass range covered by the survey, there are practically no dark galaxies in the Virgo cluster (Kent et al. 2007; Haynes et al. 2007).

In both Figs. 5 and 6 we plot the position of Malin1 (taken from Pickering et al. 1997) to show that we are sensitive to Malin1 type objects, if they existed in the Virgo cluster.

As pointed out in Sect. 2.1, the mass limit of any flux-limited HI survey depends on the line width, thus on the system's mass. Using the virial theorem, assuming a constant mass/light ratio of 4.6 (Gavazzi et al. 1996) and the best fit relation between  $R_e$  and the stellar mass (Fig. 9 and Table 1), we derive a relation between  $W$  (the line width) and the stellar mass. Using Eq. (1), we obtain the sensitivity of ALFALFA in HI mass units as  $\log(M_{\text{HI}}/M_{\odot}) = 4.25 + 0.37 \times \log M_{\text{star}} - 0.15$  (holding for non-deficient objects), where the last term represents the correction for a galaxy mean inclination of  $45^\circ$ . For less inclined galaxies the sensitivity increases, approaching  $\log(M_{\text{HI}}/M_{\odot}) = 7.5$ . The relation is plotted in Figs. 5 and 6 representing the limiting HI mass of sources in ALFALFA as a function of the stellar mass.

### 5.2. The surface brightness to stellar mass relation

One interesting issue that the ALFALFA observations of the Virgo cluster allow us to address, as outlined in the Introduction, is the question whether optical selection criteria strongly bias our knowledge of galaxies. For example, low-surface brightness objects, particularly giant, low-surface brightness, gas-rich galaxies such as Malin1, are strongly undersampled in optical catalogues, but should be detected in a radio selected sample. To explore this issue we exploit the ALFALFA sample in conjunction with the excellent (20 mag limiting magnitude and  $\sim 25.3$  mag arcsec $^{-2}$  limiting surface brightness) VCC catalogue, by comparing the optical structural parameters derived for the optically selected and for the HI selected samples. We first compare in Fig. 7 the scaling law between the optical ( $i$ -band) effective surface brightness and the stellar mass (for the subsample of the ALFALFA or VCC galaxies that we could measure on the SDSS images, i.e., all but 14 objects). The data include the HI-selected sample (filled circles & squares) and the optically-selected sample of late-type galaxies with  $m_B \leq 17$  (empty circles). The two sets of data appear to be consistent one another. The *maximum likelihood* fit to the optically selected sample is plotted together with the lines at  $\pm 2\sigma$ . The horizontal line drawn at  $\mu = 23.9$  mag arcsec $^{-2}$  is the  $i$  band mean limiting surface brightness of SDSS that we have determined as  $1\sigma$  of the sky via analysis of hundreds of images. The few measurements that lie below this line are meaningless, since they are affected by  $\sim 1$  mag arcsec $^{-2}$  uncertainty. There are at most two galaxies (VCC 307 and VCC 905, highlighted in Fig. 7) that have slightly low surface brightness for their mass, and four BCD galaxies (i.e. VCC 334, VCC 410, VCC 1313 and VCC 1437) at the opposite side of the relation, with high surface brightness for their mass. There are no others that mimic Malin1. The prototype of giant low-surface brightness galaxy, Malin1, plotted for comparison, deserves some caution. The galaxy is plotted twice (connected with a line): once at the position given by the discoverers (Bothun et al. 1987) with  $\mu_0(V) = 25.5$  mag arcsec $^{-2}$  (that we transform into  $\mu_0(i) = 25.0$  mag arcsec $^{-2}$ ) at  $10^{11} L_{\odot}$ , the other as measured on the SDSS plates. On this material the low surface brightness extended disk is not detected, instead the galaxy appears as an amorphous enhancement of high surface brightness ( $\mu_e \sim 20.5$  mag arcsec $^{-2}$ ), consistent with the inner disk detected in the HST measurement of Barth (2007). This raises the question whether other Malin1 type objects are missing in Fig. 7 because their low-surface brightness disks are below the limiting surface brightness of SDSS. These systems would wrongly count as high surface brightness systems because we would detect only their bulges or inner disks, possibly affecting the correlation between  $\mu_e$  and the stellar mass or

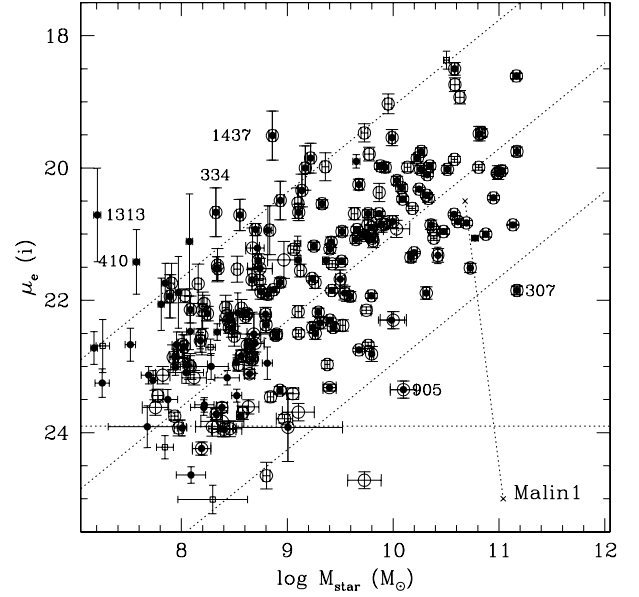


**Fig. 7.** The  $\mu_e$  vs.  $M_{\text{star}}$  relation for HI selected late-type galaxies (filled circles), optically selected late-type galaxies (empty circles) and HI selected early-type galaxies (squares). The diagonal lines represent the linear fit to the data with  $\pm 2\sigma$ . Discrepant objects are labeled with their VCC names and Malin1 is given for comparison. The horizontal line drawn at  $\mu = 23.9$  mag arcsec $^{-2}$  is the  $i$  band mean limiting surface brightness of SDSS.

even making it spurious. To make sure that this is not the case we inspected individually all galaxies on the SDSS and deeper plate material (Goldmine) and we concluded that all high surface brightness objects plotted in Fig. 7 are genuine high surface brightness spirals and BCDs, not bulges associated with missed extended disks of much lower surface brightness. The BCDs cannot be mistaken for Malin1 objects because the associated HI components have low mass and widths not exceeding  $100 \text{ km s}^{-1}$ , opposite to the HI rich and massive Malin1. Even if they were perfectly face-on, their much bluer color would discriminate BCDs from possible bulges of missed Malin1 type objects. We conclude that no Malin1-type galaxy is found in the Virgo cluster that we could have missed optically or by HI selection, in agreement with Minchin et al. (2004), who put severe upper limits on the existence of massive low surface brightness objects in the local field. Moreover we find a definite trend for the  $i$ -band surface brightness to correlate with the system mass. Extremely low surface brightness galaxies exist, but they all lie at the low mass limit of HI and optical surveys. At the limiting sensitivity of ALFALFA at Virgo ( $M_{\text{HI}} \sim 10^{7.5-8} M_{\odot}$ ) there are at most 10/185 HI sources that could possibly be identified with galaxies of lower surface brightness than the SDSS limit ( $\sim 23.9$  mag arcsec $^{-2}$ ).

### 5.3. The distribution of mass and surface brightness

Figure 8 contains histograms of the distribution of surface brightness and luminosity, both HI and optical, as derived for optical (red) and HI selected samples (blue). It may be surprising that there appears to be very little difference between the red and the blue histograms. There is indeed some excess of low surface brightness objects in the HI selected sample, represented by the 10 very faint galaxies that could not be measured on the SDSS material and are plotted as upper limits in the 25 mag arcsec $^{-2}$  bin. (Note that the 10 tidally-disrupted

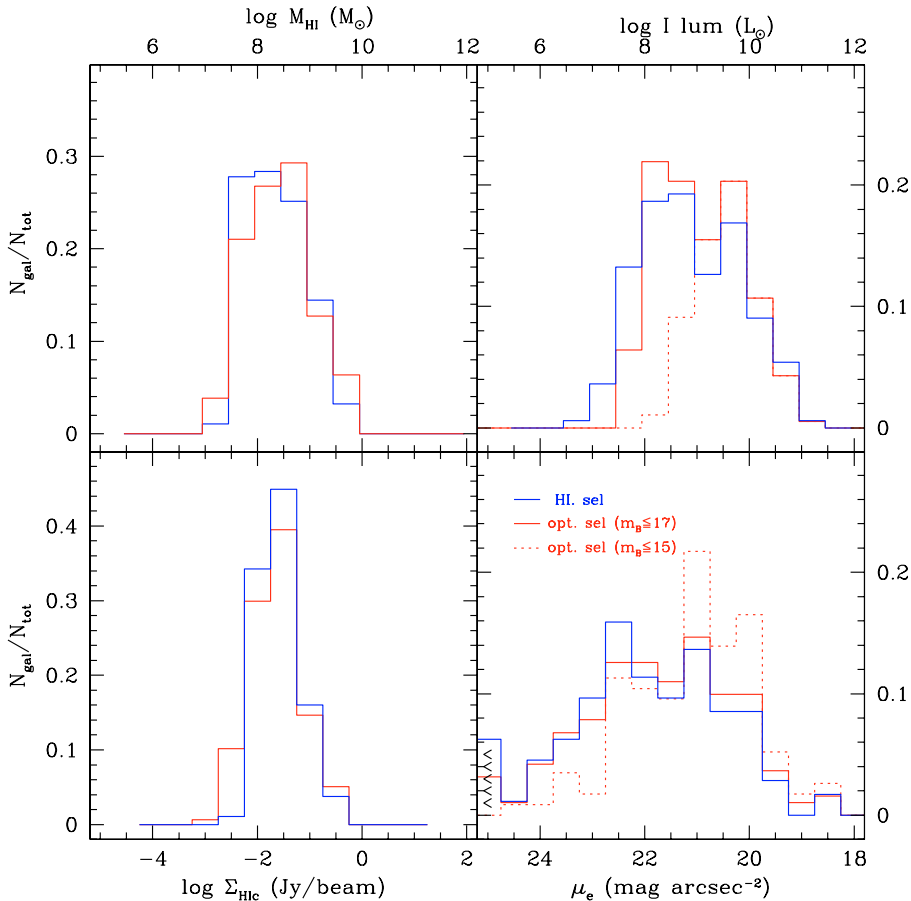


**Fig. 8.** Histograms of luminosities (*top*) and surface brightness (*bottom*) for the HI-selected (*left*) and optically-selected (*right*) samples. The distributions refer to the HI-selected sample (blue) and to the optically-selected sample limited to  $m_B \leq 17$  (solid red) and to  $m_B \leq 15$  (dotted red). Note that the bins at  $\mu_e = 25 \text{ mag arcsec}^{-2}$  represent upper limits (10 HI selected and 6 optically selected objects too faint to be measured in *i*-band).

systems were not counted among the low-surface brightness objects.) However these sources amount to less than 5% of the total number. Similarly in the optically-selected sample there are 4 VCC galaxies that could not be measured on the SDSS material. The difference is surprisingly small when we compare the HI-selected sample with the  $m_B \leq 17$  optically-selected VCC sub-sample. To show that this agreement is not at all obvious we compute the distribution also for a shallower subsample of the VCC, limited to  $m_B \leq 15$  (red dotted histogram). This time the optical (luminosity and surface brightness) distributions differ significantly from the HI-selected distributions, owing to the existence of the surface brightness vs. luminosity correlation that was investigated in Sect. 5.2 (see Fig. 7). Virgo appears just at the right distance from us to make a survey with the sensitivity of ALFALFA to match almost exactly the VCC galaxies of late-type with  $m_B \leq 17$ .

#### 5.4. Other optical structural parameters

Inspired by the analysis carried out by Cortese et al. (2007) who studied the relations between various structural parameters in their Fig. 6, we derive additional optical (*i*-band) structural parameters for the HI selected objects and for the  $m_B \leq 17$  optically selected late-type VCC sub-sample. These are the galaxy “scale” (stellar mass,  $R_e$ , luminosity or combinations) and “form” ( $\mu_e$ ,  $g - i$ ,  $C_{31}$ ) (following the terminology of Whitmore 1984). They are plotted in Fig. 9 for sources identified with galaxies selected in the blind ALFALFA HI survey (blue) and for the optically selected late-type systems from the VCC catalogue, limited to  $m_B \leq 17$  (red). The *maximum likelihood* regressions fitted to the data are plotted in Fig. 9 and reported in Table 1.

It is evident from Fig. 9 that the scaling relations well known for optically selected galaxies (e.g. color vs. mass, color vs. surface brightness,  $C_{31}$  vs. mass; Gavazzi et al. 1996; Scodreggio et al. 2002), including the Kormendy relation ( $R_e$  vs.  $\mu_e$ ), also hold true for HI selected objects. We emphasize that this result applies to galaxy members of a rich cluster such as Virgo. For example the  $\mu_e$  vs.  $M_{\text{star}}$  relation clearly shows that low surface brightness galaxies exist (and are easy to miss), but they lie mostly at the low end of the luminosity function, as discussed above. Notice in the color vs. stellar mass and color vs. surface brightness panels that the deviant points (faint-red objects) are generally dE that have structural and photometric properties intermediate between quiescent and star forming dwarfs (Boselli et al. 2008).

Furthermore the frequency distributions of the “scale” and “form” parameters are indistinguishable in HI and optically selected surveys. For example the frequency of pure disks, that have  $C_{31} < 3$  exceeds the frequency of bulge+disk systems ( $C_{31} \gg 3$ ) in both the HI- and optically-selected samples. But galaxies with  $C_{31} \gg 3$  exist in both samples. We conclude that the scaling laws that exist among the optical (*i*-band) structural parameters of disk galaxies do not differ significantly in HI and optically selected samples, although we should emphasize again that this result is limited to a rich nearby cluster.

## 6. Conclusions

By surveying the Virgo cluster, ALFALFA has provided definite evidence that: i) HI inhabits galaxies that are structurally similar to ordinary late-type galaxies; ii) their HI content can be predicted from their optical luminosity; iii) low surface brightness

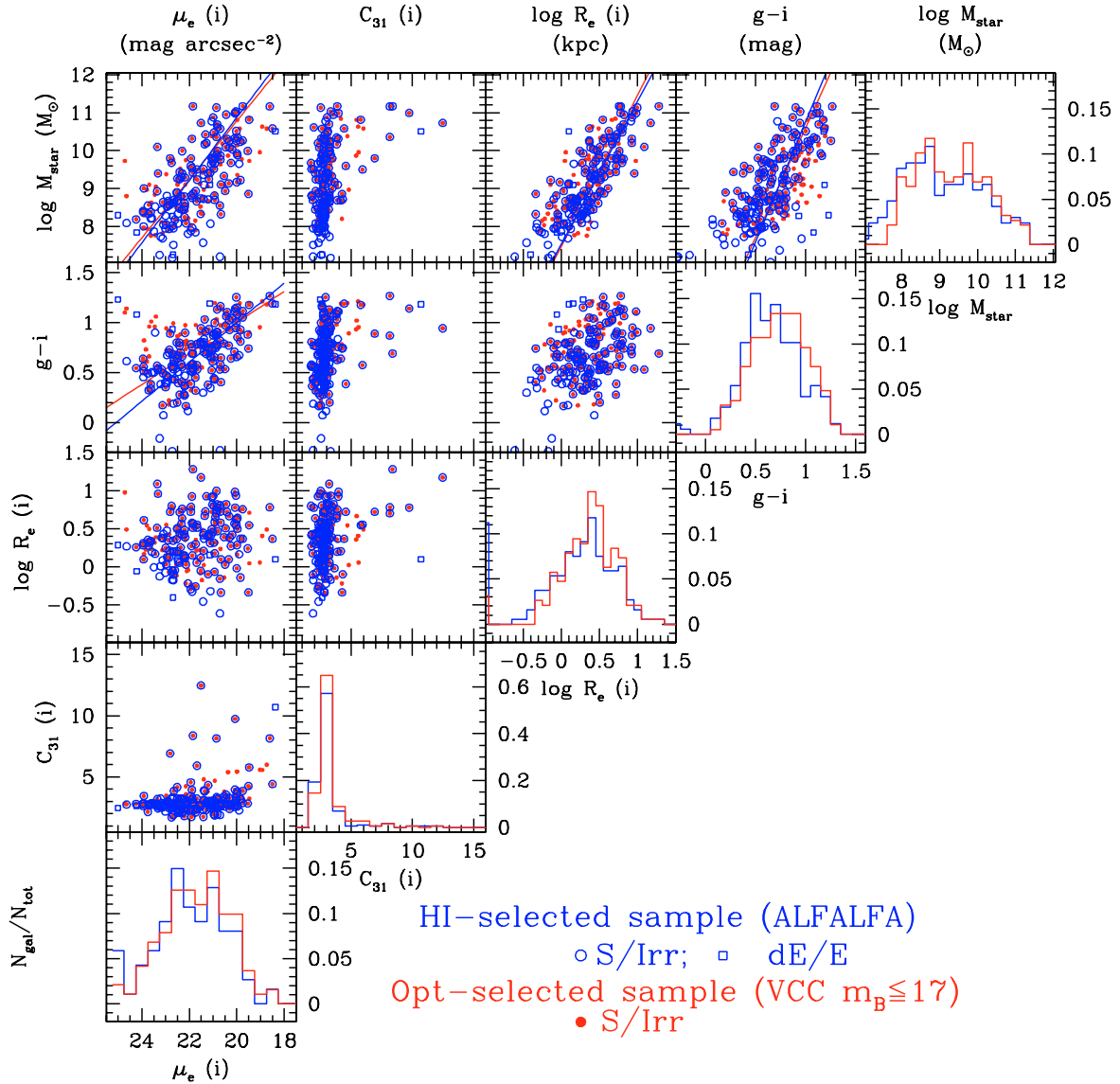


**Fig. 9.** Optical structural parameters for the HI- (blue) and optically-selected  $m_B \leq 17$  late-type galaxies (red). See text for explanation of parameters. Lines represent the *maximum likelihood* regressions fit to the data (see Table 1).

**Table 1.** *Maximum likelihood* regressions.

$y$	$x$	Condition	Figure	Slope	Intercept
$\log M_{\text{HI}}$	$\log I \text{ lum}$	$Def_{\text{HI}} < 0.6$	5	$0.563 \pm 0.002$	$3.68 \pm 0.02$
$\mu_e$	$\log M_{\text{star}}$	<i>opt</i>	7	$-1.300 \pm 0.008$	$34.01 \pm 0.08$
$\log M_{\text{star}}$	$g-i$	<i>opt</i>	9	$4.83 \pm 0.08$	$5.77 \pm 0.07$
$\log M_{\text{star}}$	$g-i$	HI	9	$4.42 \pm 0.07$	$6.34 \pm 0.05$
$\log M_{\text{star}}$	$\log R_e$	<i>opt</i>	9	$3.97 \pm 0.07$	$7.48 \pm 0.04$
$\log M_{\text{star}}$	$\log R_e$	HI	9	$3.76 \pm 0.06$	$7.54 \pm 0.04$
$\log M_{\text{star}}$	$\mu_e$	<i>opt</i>	9	$-0.769 \pm 0.005$	$26.16 \pm 0.10$
$\log M_{\text{star}}$	$\mu_e$	HI	9	$-0.825 \pm 0.006$	$27.37 \pm 0.13$
$g-i$	$\mu_e$	<i>opt</i>	9	$-0.155 \pm 0.003$	$4.10 \pm 0.07$
$g-i$	$\mu_e$	HI	9	$-0.197 \pm 0.004$	$4.94 \pm 0.08$

galaxies have low optical luminosity and contain small quantities of neutral hydrogen; iv) Malin1 type galaxies are comfortably rare objects (less than 0.5%); v) there are no “dark-galaxies” with HI masses  $M_{\text{HI}} \geq 10^{7.5-8} M_{\odot}$  (see Kent et al. 2007; and Haynes et al. 2007); vi) less than 1% of early-type galaxies contain neutral hydrogen with  $M_{\text{HI}} \geq 10^{7.5-8} M_{\odot}$  (di Serego Alighieri et al. 2007).

Once ALFALFA covers a substantial fraction of its final area, including the Virgo cluster in its full extent, a determination of the HI mass function will be obtained with unprecedented significance. We expect that the observed HI mass function of the cluster can be predicted with sufficient accuracy from the optical luminosity function of the late-type galaxies alone, accounting for the HI vs. optical luminosity relation discussed in Sect. 5.1

(Fig. 5), computed separately for normal and HI deficient objects (Kent et al., in preparation). If this is the case we expect that the faint-end slope will not differ significantly from that of the optical luminosity function of late-type galaxies, i.e. flatter than the halo mass function predicted theoretically from the CDM cosmology.

*Acknowledgements.* We thank L. Cortese and C. Bonfanti for precious hints and useful discussions. This research has made use of the Goldmine database.

Funding for the Sloan Digital Sky Survey (SDSS) and SDSS-II has been provided by the Alfred P. Sloan Foundation, the Participating Institutions, the National Science Foundation, the US Department of Energy, the National Aeronautics and Space Administration, the Japanese Monbukagakusho, and the Max Planck Society, and the Higher Education Funding Council for England. The SDSS Web site is <http://www.sdss.org/>. The SDSS is managed by the Astrophysical Research Consortium (ARC) for the Participating Institutions. The Participating Institutions are the American Museum of Natural History, Astrophysical Institute Potsdam, University of Basel, University of Cambridge, Case Western Reserve University, The University of Chicago, Drexel University, Fermilab, the Institute for Advanced Study, the Japan Participation Group, The Johns Hopkins University, the Joint Institute for Nuclear Astrophysics, the Kavli Institute for Particle Astrophysics and Cosmology, the Korean Scientist Group, the Chinese Academy of Sciences (LAMOST), Los Alamos National Laboratory, the Max-Planck-Institute for Astronomy (MPIA), the Max-Planck-Institute for Astrophysics (MPA), New Mexico State University, Ohio State University, University of Pittsburgh, University of Portsmouth, Princeton University, the United States Naval Observatory, and the University of Washington.

## References

- Abadi, M. G., Moore, B., & Bower, R. G. 1999, *MNRAS*, 308, 947  
 Adelman, J., et al. 2007, *Ops* (in press)  
 Auld, R., Minchin, R. F., Davies, J. I., et al. 2006, *MENS*, 371, 1617  
 Barth, A. J. 2007, *AJ*, 133, 1085  
 Bell, E. F., McIntosh, D. H., Katz, N., et al. 2003, *ApJ*, 149, 289  
 Binggeli, B., Sandage, A., & Tammann, G. 1985, *AJ*, 90, 1681  
 Binggeli, B., Popescu, C., & Tammann, G. 1993, *A&AS*, 98, 275  
 Böhringer, H., Briel, U. G., Schwarz, R. A., et al. 1994, *Nature*, 368, 828  
 Blanton, M. R., Hogg, D. W., Bahcall, N. A., et al. 2003, *ApJ*, 592, 819  
 Boselli, A., & Gavazzi, G. 2006, *PASP*, 118, 517  
 Boselli, A., Gavazzi, G., Donas, J., & Scodreggio, M. 2001, *AJ*, 121, 753  
 Boselli, A., Lequeux, J., & Gavazzi, G. 2002, *A&A*, 384, 33  
 Boselli, A., Boissier, S., Cortese, L., & Gavazzi, G. 2008, *ApJ*, in press  
 Briggs, F. H. 1997, *ApJ*, 484, L29  
 Cortese, L., et al. 2007, *MNRAS*, in press  
 de Vaucouleurs, G. 1977, in *Evolution of Galaxies and Stellar Populations*, ed. R. Larson, & B. Tinsley (New Haven: Yale University Observatory), 43  
 Disney, M. 1976, *Nature*, 263, 573  
 Disney, M., & Phillipps, S. 1987, *Nature*, 329, 203  
 Gavazzi, G., Pierini, D., & Boselli, A. 1996, *A&A*, 312, 397  
 Gavazzi, G., Boselli, A., Scodreggio, M., Pierini, D., & Belsole, E. 1999, *MNRAS*, 304, 595  
 Gavazzi, G., Zibetti, S., Boselli, A., et al. 2001, *A&A*, 372, 29  
 Gavazzi, G., Boselli, A., Donati, A., Franzetti, P., & Scodreggio, M. 2003, *A&A*, 400, 451  
 Gavazzi, G., Boselli, A., van Driel, W., & O'Neil, K. 2005, *A&A*, 429, 439  
 Giovanelli, R., & Haynes, M. 1985, *ApJ*, 292, 404  
 Giovanelli, R., Haynes, M., Kent, B., et al. 2005, *AJ*, 130, 2598  
 Giovanelli, R., Haynes, M., Kent, B., et al. 2007, *AJ*, 133, 2569  
 Haynes, M., & Giovanelli, R. 1984, *AJ*, 89, 758  
 Haynes, M. P., Giovanelli, R., & Kent, B. R. 2007, *ApJ*, 665, L19  
 Hayward, C. C., Irwin, J. A., & Bregman, J. N. 2005, *ApJ*, 635, 827  
 Impey, C., & Bothun, G. 1989, *ApJ*, 341, 891  
 Jenkins, A., Frenk, C. S., White, S., et al. 2001, *MNRAS*, 321, 372  
 Kent, B., Giovanelli, R., Haynes, M., et al. 2007, *ApJ*, 665, L15  
 Kormendy, J. 1985, *ApJ*, 295, 73  
 Kovac, K. 2007, Ph.D. Thesis, University of Groningen  
 Masters, K. L., Giovanelli, R., & Haynes, M. 2004, *ApJ*, 607, 115  
 Masters, K., Springob, C. M., Haynes, M. P., et al. 2006, *ApJ*, 653, 861  
 Meyer, M. J., Zwaan, M. A., Webster, R. L., et al. 2004, *MNRAS*, 350, 1195  
 Minchin, R. F., Disney, M. J., Boyce, P. J., et al. 2003, *MNRAS*, 346, 787  
 Minchin, R. F., Disney, M. J., Parker, Q. A., et al. 2004, *MNRAS*, 355, 1303  
 Pickering, T. E., Impey, C. D., van Gorkom, J. H., & Bothun, G. D. 1997, *AJ*, 114, 1858  
 Press, W. H., & Schechter, P. 1974, *ApJ*, 187, 425  
 Roberts, M. S., & Haynes, M. P. 1994, *ARA&A*, 32, 115  
 Rosenberg, J. L., & Schneider, S. E. 2002, *ApJ*, 567, 247  
 Sabatini, S., Davies, J., Scaramella, R., et al. 2003, *MNRAS*, 341, 981  
 Scodreggio, M., Gavazzi, G., Franzetti, P., et al. 2002, *A&A*, 384, 812  
 di Serego Alighieri, S., et al. 2007, *A&A*, 474, 851  
 Springob, C. M., Giovanelli, R., & Haynes, M. 2005, *ApJ*, 621, 215  
 Warren, B. E., Jerjen, H., & Koribalski, B. S. 2006, *AJ*, 131, 2056  
 Whitmore, B. C. 1984, *ApJ*, 278, 61  
 Zwaan, M. A., Briggs, F. H., & Sprayberry, D. 2001, *MNRAS*, 327, 1249  
 Zwaan, M. A., Staveley-Smith, L., Koribalski, B. S., et al. 2003, *AJ*, 125, 2842  
 Zwaan, M. A., Meyer, M. J., Staveley-Smith, L., et al. 2005, *MNRAS*, 359, L30